# Catalytic Partial Oxidation of Methane in a High-Temperature Reverse-Flow Reactor

**Dirk Neumann and Götz Veser**
Dept. of Chemical Engineering, University of Pittsburgh, Pittsburgh, PA 15261

and

Max-Planck-Institut für Kohlenforschung, D-45470 Mülheim a.d. Ruhr, Germany

*DOI 10.1002/aic.10284*
*Published online in Wiley InterScience (www.interscience.wiley.com).*

*The production of hydrogen and synthesis gas (syngas) from methane is a key technology for the twenty-first century. It is currently performed predominantly by steam reforming of methane. An alternative reaction route is the direct catalytic partial oxidation of methane (CPOM) at high-temperature, short contact time conditions, which proceeds autothermally over noble metal catalysts. However, syngas yields are limited at autothermal operation by a complex interplay of total and partial oxidation reactions. We demonstrate that these limitations can be overcome through dynamic heat integration in a catalytic reverse-flow reactor. The efficient heat integration in this reactor type leads to strongly increased syngas yields; that is, it effectively converts sensible heat into chemical energy. Furthermore, even shorter contact times can be achieved without yield losses, allowing for even more compact reactors or further increased reactor throughput. The combination of short contact time catalysis with dynamic heat integration therefore appears ideally suited for small-scale and decentralized syngas and hydrogen production.*
 *AIChE J,* 51: 210–223, 2005
*Keywords: catalytic partial oxidation of methane, synthesis gas (syngas), heat integration, reverse-flow reactor, short contact time catalysis*

## Introduction

The exploitation of methane as an alternative to crude oil is gaining increased attention in recent years, which is primarily attributed to the large world reservoirs of natural gas (largely methane with minor amounts of higher hydrocarbons and other trace components, depending on the location) that are currently being vastly underutilized. Furthermore, biomass offers a potentially significant renewable source of methane,[1,2] and vast amounts of methane are bound in methane hydrates at the bottom of the world's oceans as well as in surface layers in the arctic region.[3] However, for an efficient and economically feasible use of these resources, new concepts and processes for methane utilization need to be developed.

In addition to being a comparatively clean source of energy (attributed to the large heat of combustion relative to $CO_2$ formed), methane can also be used as a source of hydrogen and for the production of liquid chemicals such as methanol and synthetic fuels [in so-called gas-to-liquid (GTL) processes]. For this purpose, methane can be converted either directly (that is, in a one-step process) or indirectly (that is, by one or more intermediate steps). Although the direct conversion is still studied at a fundamental level[4] and so far results in unacceptably low reaction yields, the indirect process is applied on a large scale in industrial practice. Here, methane is converted in a primary step to synthesis gas ("syngas," a mixture of $H_2$ and CO), followed by different processes to manufacture the desired chemical.[5]

Industrially, syngas is typically produced by steam reform-

Correspondence concerning this article should be addressed to G. Veser at gveser@pitt.edu

ing of methane (SRM), in which methane is converted with water over Ni catalysts in a strongly endothermic reaction to yield CO and $H_2$ in a molar ratio of 1:3:

$$CH_4 + H_2O \rightarrow CO + 3\,H_2 \qquad \Delta H_r = +206\ \text{kJ/mol}$$

The process is conducted in large tubular reformers to achieve high temperatures that are thermodynamically necessary for good syngas yields, making SRM a major energy consumer. For most downstream processes (such as methanol and Fischer–Tropsch synthesis), however, the desired $H_2$/CO ratio is 2.0. Therefore, the steam reformer is typically followed by additional water gas shift stages in the process scheme to adjust the $H_2$/CO ratio to the desired value

$$CO + H_2O \rightarrow CO_2 + H_2 \qquad \Delta H_r = -41\ \text{kJ/mol}$$

Because the residence times inside the reactors are in the order of 1 s, large reactor volumes are necessary for high throughputs.

A promising alternative technology that has received much attention during the last decade is catalytic partial oxidation of methane (CPOM) at high temperature and short contact time conditions.[6] In this process, methane is converted with oxygen or air over noble metal catalysts to syngas in a simple, one-step reaction

$$CH_4 + 0.5O_2 \rightarrow CO + 2H_2 \qquad \Delta H_r = -37\ \text{kJ/mol}$$

The system is characterized by high autothermal temperatures exceeding 1000°C, which result in very high reaction rates and thus very high space-time yields can be achieved. Thus, in principle, the process has several advantages over SRM: The exothermicity of the reaction allows autothermal reactor operation; that is, it renders expensive external heating unnecessary. Furthermore, the very high reaction rates allow for unusually compact reactors. The CPOM process therefore seems ideally suited to enable a more efficient use of methane and natural gas resources, especially in remote locations or for small-scale, decentralized and for mobile applications.

### *Thermodynamic considerations*

Thermodynamic calculations for methane/air mixtures show that the high autothermal temperatures in excess of 1000°C are in fact necessary to achieve optimum syngas yields. (*Autothermal temperature* denotes the temperature that a reaction system reaches autonomously, that is, without additional heating or specific reactor design or operating measures for heat integration. It is a function of the reactor feed composition, the reaction extent, and possible heat losses from the reactor.) These high temperatures, however, cannot result from the mild exothermicity of the partial oxidation route ($\Delta H_r = -37$ kJ/mol), which yields an adiabatic temperature increase of only $\Delta T_{ad} \sim 250$ K. Instead, they are attributed to combustion (that is, total oxidation) of some of the methane feed, which is a highly exothermic reaction ($\Delta H_r = -800$ kJ/mol), with an adiabatic temperature increase of $\Delta T_{ad} \sim 2000$ K. The reaction yield is thus ultimately determined by a complex interplay between partial and total oxidation reactions: whereas the combustion of methane results in high temperatures, these high temperatures shift the reaction equilibrium toward the partial oxidation route. Total oxidation thus has a beneficial effect on reaction equilibrium, whereas the formation of total oxidation products at the same time, by definition, also reduces syngas selectivities. Overall, this interplay limits attainable partial oxidation yields under autothermal operation.

To quantify these limitations at autothermal reactor operation, calculated syngas compositions at adiabatic and optimum equilibrium temperatures as a function of the $CH_4/O_2$ ratio in a $CH_4$–air system are shown along with the respective temperatures in Figure 1. Data points labeled "adiabatic" represent selectivities and conversions at the adiabatic temperature of the respective methane/air mixture. Data points labeled "optimum" represent equilibrium selectivities and conversions at temperatures where a maximum in the respective selectivity or conversion is achieved. The initial state of the system (that is, the reactor feed) is at room temperature ($T = 298$ K).

Clearly, thermodynamics allow for optimum syngas yields (of virtually 100%) at temperatures around 1050°C and at the stoichiometric $CH_4/O_2$ ratio for partial oxidation of 2.0. However, autothermal operation reduces the maximum attainable syngas selectivities by about 10–20% and methane conversions by about 20% compared to optimum temperature conditions. Although these thermodynamic calculations obviously neglect the influence of reaction kinetics on process yields, they nevertheless indicate that temperatures in excess of adiabatic temperatures are beneficial for syngas yields, and reactor concepts to raise adiabatic process temperatures are thus imperative for an efficient realization of the CPOM process.

### *Heat integration*

Initial investigations of the CPOM reaction route by Hickman and Schmidt[7] already showed that preheating of the reactants indeed results in increased syngas yields. Although external preheating can be easily realized, it is expensive and ultimately creates additional process emissions. A much more economic way is to integrate the sensible heat leaving the reaction zone in a multifunctional reactor concept.[8,9] Friedle and Veser[10] previously reported enhanced partial oxidation selectivities when performing CPOM in a countercurrent heat-exchange reactor. A much more efficient heat integration, however, can be achieved in a reverse-flow reactor (RFR).[11] In this reactor concept, periodic switching of the flow direction of the gases through the reactor results in a very efficient internal regenerative heat exchange, which makes this concept particularly suitable for weakly exothermic reactions.

In a typical RFR configuration, inert packing materials, so-called inert zones, are placed on either side of the reaction zone and act as regenerative heat exchangers in addition to the catalyst bed. Figure 2 shows a schematic of the temperature profile along the reactor axis in an RFR at operating conditions. Cold reactants enter the catalyst bed and react exothermically on the catalyst surface. Hot product gases exit the reaction zone and exchange heat with the inert zone downstream of the catalyst (Figure 2, panel 1, $t = 0$), which is therefore heated up. The gas flow through the reaction tube is reversed, and cold reactants entering the reactor are heated up by the hot inert zone, which is now located upstream of the catalyst. The reactants enter the

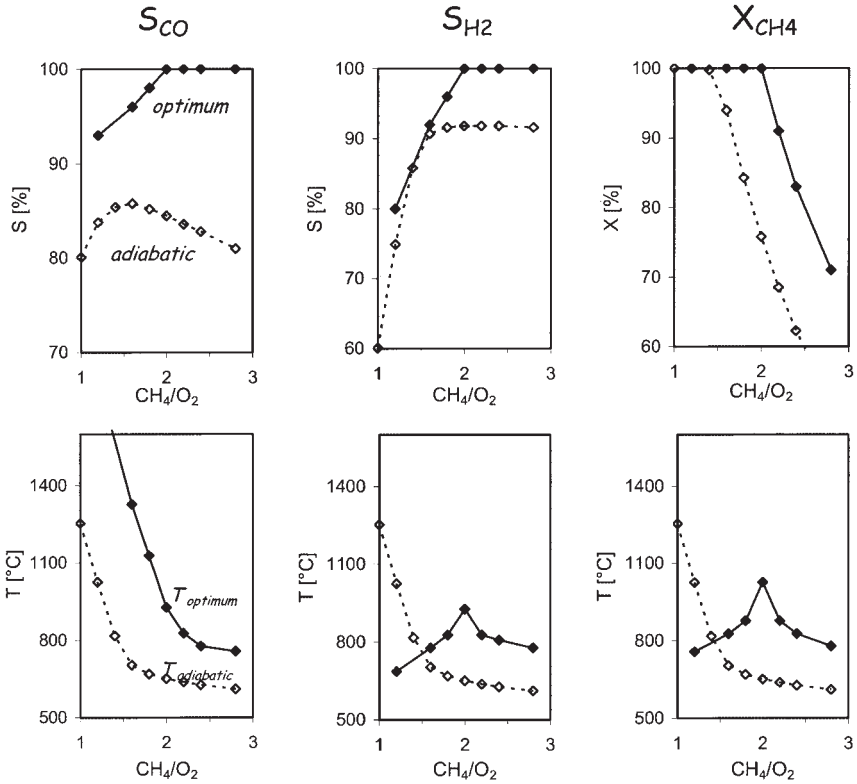


**Figure 1. Thermodynamic calculations.**

Adiabatic (dashed lines) and optimum (solid lines) CO and $H_2$ selectivities ($S_{CO}$, left; $S_{H2}$, middle) as well as $CH_4$ conversions ($X_{CH4}$, right; top row); corresponding optimum temperatures (solid lines) and adiabatic temperatures (dashed lines; bottom row).

catalyst bed at an elevated temperature, which adds to the heat of reaction and leads to an overall increase of the catalyst temperature (Figure 2, panel 2; previous temperature profiles are represented by the dashed line, current ones by the solid lines). Hot product gases exit the reaction zone and exchange heat with the cold inert zone downstream of the catalyst bed. The continuous heat exchange now leads to a cooling of the heat reservoir upstream and a heating of the heat reservoir downstream of the catalyst (Figure 2, panels 3–4).

To prevent the catalyst temperature from dropping once the inert zone upstream of the catalyst has been cooled down, the flow is reversed periodically (with $t = \tau/2$, where $\tau/2$ denotes the duration of one half-period, that is, the time during which the gas flows in one direction only), resulting in a very efficient heat integration. If the flow reversals are repeated frequently enough, the characteristics (temperatures, concentration profiles) of a full cycle are identical to the preceding one and the system has reached the so-called periodic steady state.

Pioneering work concerning reverse-flow reactor operation has been performed by Matros and coworkers,[11-13] which resulted in the industrial implementation of this technique for $SO_2$ oxidation.[12] The functional principle of the RFR was later elegantly explained by Eigenberger and coworkers,[14,15] who

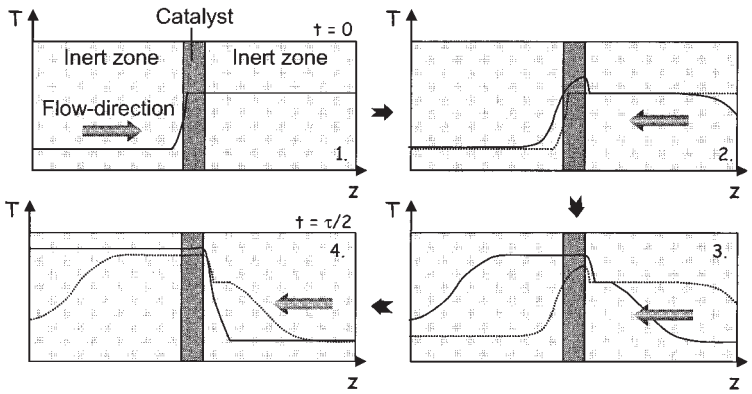


**Figure 2. Schematic of regenerative heat exchange in an RFR.**

Temperature profiles along the reactor axis $z$ during one semicycle (clockwise from top left).

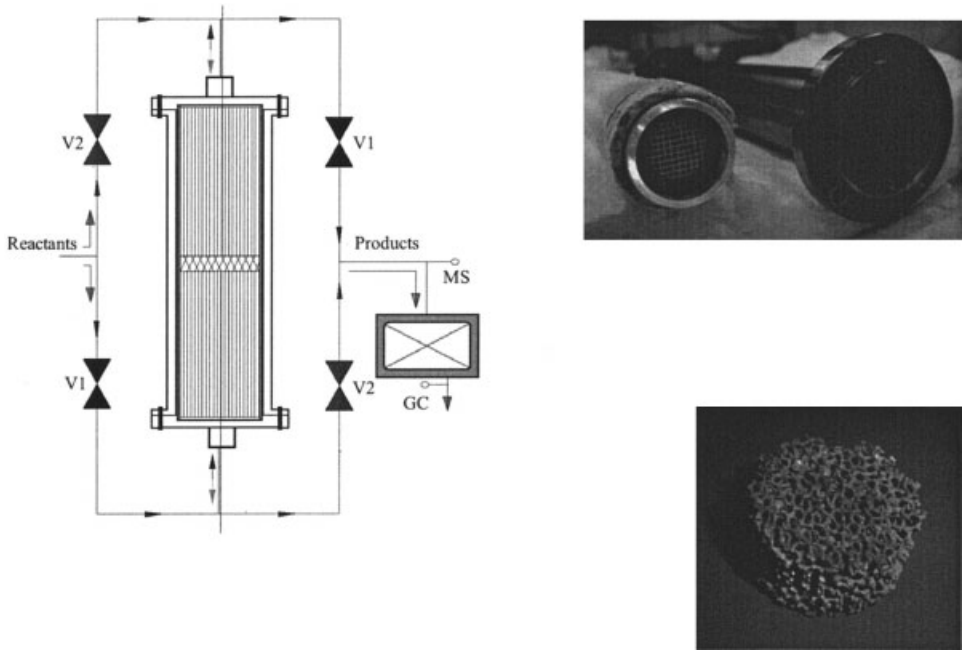


**Figure 3. RFR system (left) and photos of the laboratory reactor (right top) as well as the Pt-coated alumina foam catalyst used in the experiments (right bottom).**

studied this reactor concept for the incineration of waste gases and more recently for the catalytic dehydrogenation of ethylbenzene.[16]

To date, only one experimental study investigating CPOM in an RFR has been published. Blanks et al.[17] investigated the conversion of natural gas with air in an adiabatic pilot-plant–scale reactor, using a Ni on alumina methane reforming catalyst. Furthermore, numerical studies were performed by De Groote and Froment,[18] Gosiewski et al.,[19] and Gosiewski.[20] In all of these studies, the authors concluded that the RFR is not a suitable reactor configuration for CPOM because of the formation of a heat wave, which leads to unacceptably high temperatures. In the following, we will demonstrate that this is not necessarily the case and that reverse-flow operation in fact yields strong process improvements in CPOM.

## Experimental

### *Setup*

Figure 3 shows a schematic of the experimentally used RFR system. Switching of the flow direction through the reaction tube is accomplished with two sets of two magnetically operated valves (V1 and V2), which are positioned parallel in front of and behind the reactor. By keeping two diagonally positioned valves open while closing the remaining two, the flow direction of the gases through the reactor is determined. Reversing the flow direction is accomplished by closing the open valves and opening the closed ones.

The reactor design is based on knowledge gained from previous steady-state experiments in a quartz-glass tube as well as a countercurrent heat-exchange reactor.[10] It consists of a high-temperature steel housing with an inner quartz-glass tube into which the catalyst and the inert zones are inserted (see Figure 3, right top). This setup takes into account that, although standard steel does not withstand the high temperatures during reactor operation, typical (highly alloyed) high-temperature steels become catalytically active, degrading the reactor and reaction yields. At the same time, integration of the reactor tube into the RFR system necessitates a thermally and mechanically stable connection. Several reactor configurations were tested until these guidelines were adequately met. The monolithic inert zones and catalysts are rolled in alumina paper to avoid a bypass between the ceramic and the quartz tube. The glass tube is then wrapped in several layers of alumina cloth and inserted into the steel housing. Finally, the steel housing is embedded into an insulation cloth to minimize heat losses.

The catalysts used in the experiments are Pt-coated alumina foam monoliths [45 ppi (pores per linear inch); Vesuvius High-Tech Ceramics], which are prepared from $H_2PtCl_6$ solutions by standard impregnation and calcination procedures, typically yielding about 5–6 wt % Pt. The inert packings (so-called inert zones) are made from cordierite extruded monoliths [350 cpi (cells per square inch); Corning] and are placed before and after the catalyst bed to act as radiation shields in addition to solid-state heat reservoirs for the regenerative heat exchange at dynamic reactor operation.

Temperatures are measured with type K thermocouples on either side of the catalyst bed. Both thermocouples are movable and thus allow measurement of temperature profiles in the (extruded) inert zones along the reactor axis. Because of the irregular foam structure of the catalyst support, however, it is not possible to measure temperature profiles inside the monolithic catalyst itself.

The pressure is measured at the reactor inlet and outlet using pressure transmitters (Jumo 4AP-30). Flow of methane (4.0 grade, Valley National Gas) and air (0.1 grade, VNG) is controlled by standard mass flow controllers (MKS 1179A).

Product gases are analyzed using a mass spectrometer (Balzers Quadstar GSD 300) for qualitative, time-resolved mea-

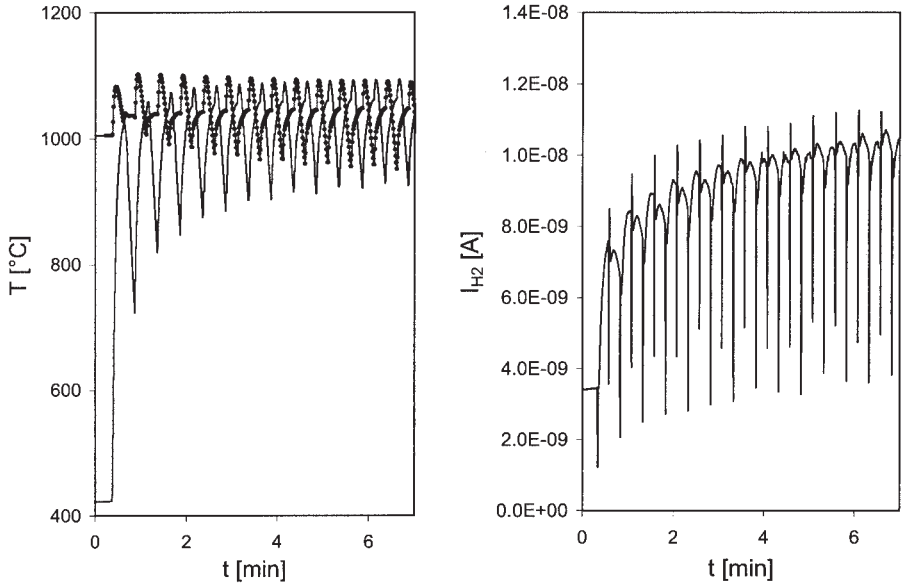


**Figure 4. Temperatures at the catalyst entrance and exit (left) as well as $H_2$ concentrations at the reactor exit (right) during initial 7 min of transition from steady-state to dynamic RFR operation.**

surements, and a double-oven gas chromatographic system (two Shimadzu GC-14B systems) for quantitative measurements. The GC system determines the concentrations of all major components $CH_4$, $O_2$, $N_2$, $H_2$, $H_2O$, CO, and $CO_2$. Using this setup, atom balances for all atomic species close in a typical run to better than 2%. Selectivities toward partial oxidation products as well as methane conversions are calculated using molar concentrations of the product gases. Additionally, a vessel with a 2-L volume can be connected in series before the GC. This ensures an appropriate mixing of the nonstationary product gases and allows for a simple and reliable quantitative measurement of mean component concentrations for a full cycle during dynamic reactor operation.

Reactor operation (switching of valves, temperature, and pressure readings) and data processing are fully computer controlled (LabView 6.i software).

For a direct comparison of the results at reverse-flow operation with results from a conventional reactor, the same reactor setup is used for steady-state experiments by omitting the switching of flow direction. In this way, it is ensured that all differences between steady-state results and results at reverse-flow conditions are exclusively attributed to differences in reactor operation rather than differences in the experimental setup.

## Results

### *Dynamic reactor operation*

Dynamic reactor operation results in a non-steady-state heat integration. As a consequence, temperature and concentration profiles are time dependent and repeat periodically with the cycling time of flow reversal $\tau$. After the initial start-up phase, the so-called periodic steady state has been reached once temperature and concentration profiles during a cycle are identical to the preceding and following cycles.

An example for the approach of temperatures measured on either side of the catalyst bed (left graph) as well as $H_2$ concentrations measured at the outlet of the reactor (right) toward periodic steady-state conditions is shown in Figure 4. During the initial 30 s, the reactor is operated at steady-state conditions and temperatures and concentrations remain constant. Then, periodic flow reversal begins and repeat every 15 s (that is, $\tau/2 = 15$ s). Characteristic temperature curves develop at the catalyst entrance and exit, with average temperatures being virtually unchanged from exit temperatures at steady-state operation. In contrast to that, $H_2$ concentrations show a strongly increasing trend in reverse-flow mode. Furthermore, it can also be observed (qualitatively) from this figure that after

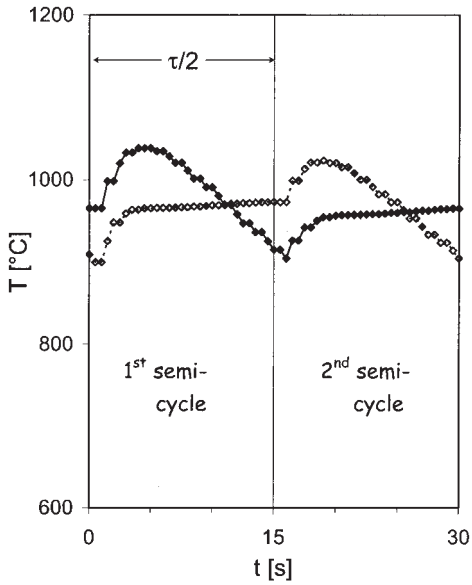


**Figure 5. Time-dependent temperatures measured on either side of the catalyst bed for two semi-cycles at periodic steady state.**

$CH_4/O_2 = 2.0$, $\tau/2 = 15$ s, $\dot{V} = 3$ slm.

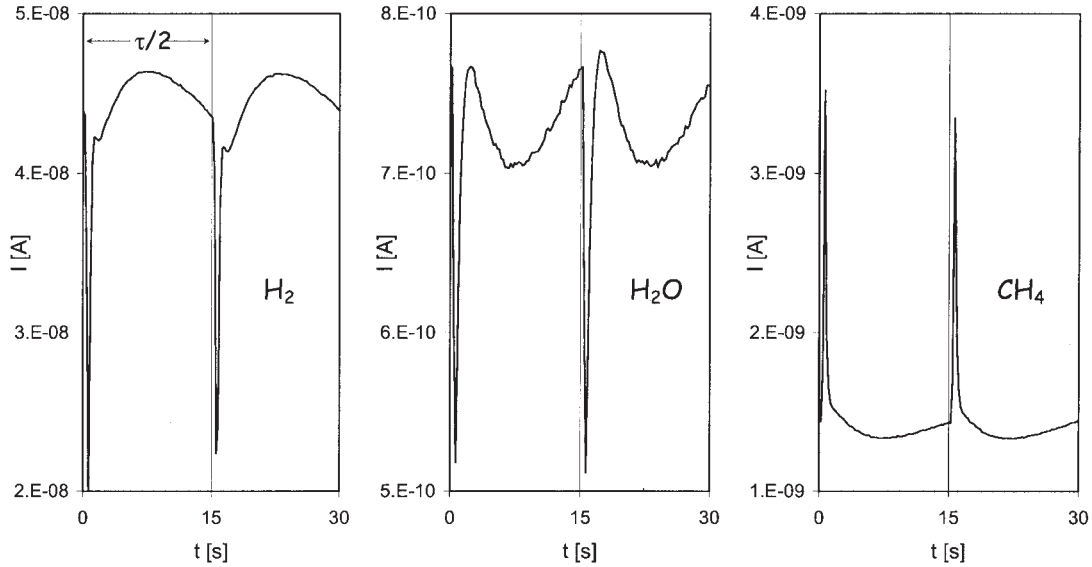


**Figure 6. $H_2$ (left), $H_2O$ (middle), and $CH_4$ (right) concentrations during 2 semicycles at periodic steady state.**
$\tau/2 = 15$ s, $\dot{V} = 4$ slm, $CH_4/O_2 = 2.6$.

only 7 min (that is, 13 cycles), the periodic steady state has already been approached to a large degree. At typical operating conditions, periodic steady state was attained after about 30 min.

Figure 5 shows the progression of temperatures measured at the catalyst entrance and exit during two semicycles in periodic steady state [flow rate $\dot{V} = 3$ slm (standard liters per minute); semicycling period $\tau/2 = 15$ s, $CH_4/O_2 = 2.0$]. The position of the catalyst entrance and exit is defined relative to the gas flow, which changes direction through the reaction tube every semicycle. The stationary thermocouples positioned at either end of the catalyst bed therefore measure the entrance temperature during one half-period and the exit temperature during the next half-period (and vice versa). The two semicycles shown in Figure 5 have been marked "1st semicycle" and "2nd semicycle," respectively. Solid diamonds represent catalyst entrance temperatures in the first semicycle, whereas open diamonds represent temperatures at the exit of the reaction zone. In the second semicycle, the relative positions switch and open squares display entrance temperatures, whereas solid squares represent exit temperatures.

Catalyst entrance temperatures proceed through a maximum within the first couple of seconds after flow reversal, which is followed by a continuous decrease. Catalyst exit temperatures initially show a strong increase that flattens during the course of the semicycle.

The temperature curve at the catalyst entrance is a result of dynamic heat integration in the RFR. Temperatures are determined by the heat of reaction, the feed gas temperature, convective cooling, and heat losses from the reactor. In periodic steady state, the amount of heat accumulated in the inert zone downstream of the catalyst during one semicycle has a maximum value at the point of flow reversal (end of semicycle). After flow reversal, cold reactants entering the reactor are heated up by the heat reservoir—which is now upstream of the reaction zone—before entering the catalyst bed. During the semicycle, the feed gas maintains a maximum temperature for a certain time, which depends on the amount of heat accumulated in the inert zone. The catalyst entrance temperature increases continuously during this time because the preheated feed gas is now providing additional heat on top of the heat of reaction. Once the heat reservoir is empty, the feed gas temperature decreases and consequently results in a decrease of the catalyst entrance temperature.

In contrast to catalyst entrance temperatures, exit temperatures are not as dependent on the heat integration. A strong temperature increase within the first few seconds is followed by an almost constant temperature during the remaining part of the semicycle. Initially, the relatively cold monolith exit zone (which was the catalyst entrance in the preceding semicycle) is heated by hot effluent product gases, which leads to the observed temperature increase. Thereafter, catalyst exit temperatures remain essentially constant and are not influenced by varying catalyst entrance temperatures. This observation already indicates that, to some extent, sensible heat is converted into chemical energy (that is, into an increase in syngas yields), given that a change in catalyst entrance temperature does not have an effect on catalyst exit temperatures.

Time-dependent product gas concentrations are measured qualitatively with an MS at the outlet of the RFR system. The location of the MS allows measurement of the product gas stream independent of the flow direction through the reactor (see Figure 3). Therefore, concentration curves repeat periodically with $\tau/2$. As an example, Figure 6 shows representative curves for partial oxidation products ($H_2$), total oxidation products ($H_2O$), and reactant concentrations ($CH_4$) during two semicycles ($\tau/2 = 15$ s, $\dot{V} = 4$ slm, $CH_4/O_2 = 2.0$).

All concentrations show a distinct spike immediately after every flow reversal. Thereafter, $H_2$ concentration exhibits a broad convex curve, whereas $H_2O$ and $CH_4$ concentrations show a broad concave curve. The shapes of these curves thus indicate that instantaneous reaction selectivities display a maximum about halfway through a semicycle, after which they rapidly decline. The achievement of optimal process yields can

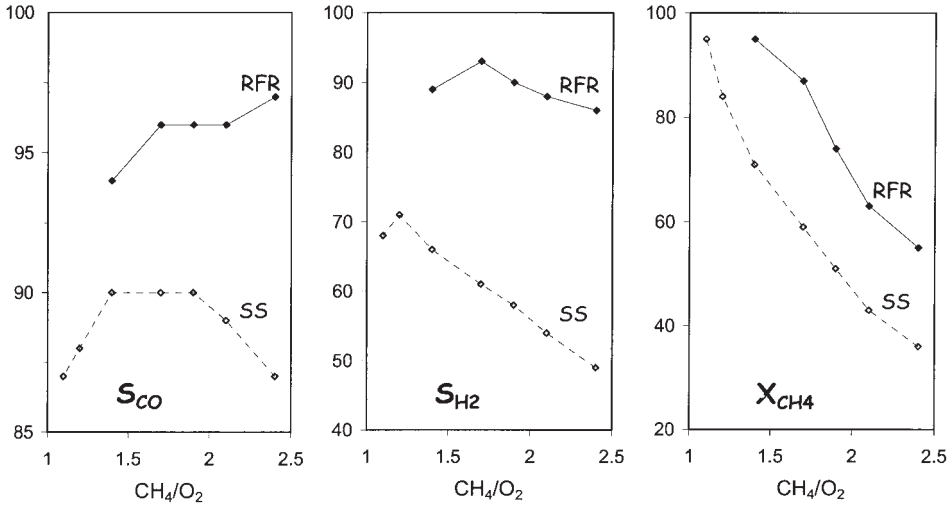


**Figure 7. CO selectivities ($S_{CO}$, left), $H_2$ selectivities ($S_{H2}$, middle), and $CH_4$ conversions ($X_{CH4}$, right) as a function of the $CH_4/O_2$ ratio for steady-state (SS, dotted lines) and RFR (solid lines) operation.**

$\dot{V}$ = 4 slm, $\tau/2$ = 15 s.

thus be expected to be dependent on the duration of the semicycle in reverse-flow operation (see below).

Although the "broad" features of the curves are a direct result of the heat integration on the reaction kinetics, the sharp spikes after each flow reversal occur as a result of a flushing out of unconverted reactants in front of the catalyst bed. In a large-scale technical RFR, a so-called flushing phase with an inert gas before every semicycle prevents reactants from exiting the system after flow reversal. This can be a very important aspect, say, for downstream processes, where unconverted reactants of the first process can lead to selectivity losses or even to poisoning of the catalyst used in the following processes. Furthermore, yield losses can be substantial if large reactor volumes are used. However, in the investigated short contact time system, the very high throughputs and the compactness of the reactor result in a negligible effect on global yields. This omission of a flushing phase thus greatly simplifies reverse-flow operation for this and similar high-temperature, short contact time catalytic systems for applications where contamination of the product gases with trace amounts of unconverted reactants is tolerable.

In the following, selectivities and methane conversions as well as temperatures will be displayed as averages of a full cycle at periodic steady-state conditions. This facilitates the comparison between true reactor performance at (dynamic) reverse-flow and (conventional) steady-state conditions.

### *Variation of the feed gas composition*

CPOM is characterized by a complex interplay between partial and total oxidation reactions. The stoichiometric point for partial oxidation is at a $CH_4/O_2$ ratio of 2.0 and for total oxidation at 0.5. This makes the $CH_4/O_2$ ratio of the feed gas a decisive parameter for influencing reaction selectivities.

Figure 7 shows partial oxidation selectivities and methane conversions for different $CH_4/O_2$ ratios in the RFR in comparison to conventional steady-state (SS) reactor operation (at a flow rate $\dot{V}$ = 4 slm; semicycle period $\tau/2$ = 15 s). Oxygen conversions are always close to 100% and are therefore not shown.

CO selectivities exhibit very little variation for all $CH_4/O_2$ ratios (86–90% in the conventional process and 94–97% in RFR operation). $H_2$ selectivities show a maximum at a $CH_4/O_2$ ratio of 1.2 in steady-state operation ($S_{H2}$ = 71%) and at a $CH_4/O_2$ ratio of 1.7 in RFR operation ($S_{H2}$ = 93%). Methane conversions increase continuously with decreasing $CH_4/O_2$ ratios (from 36% at $CH_4/O_2$ = 2.4 to 95% at $CH_4/O_2$ = 1.1 in the stationary process and from 55% at $CH_4/O_2$ = 2.4 to 95% at $CH_4/O_2$ = 1.4 in RFR operation). Overall, RFR operation thus results in a pronounced increase in syngas yields over the whole range of $CH_4/O_2$ ratios investigated.

Figure 8 shows the corresponding temperature measurements. RFR temperatures shown are mean catalyst entrance and exit temperatures averaged over a full cycle as well as maximum temperatures (at the catalyst entrance and exit) during that cycle. Both the dynamic and the steady state process exhibit virtually constant temperatures over a broad range of $CH_4/O_2$ ratios ($T_{entrance} \sim 500$°C, $T_{exit} \sim 1000$°C in steady state; mean $T \sim 1050$°C and maximum $T \sim 1120$°C in RFR operation). A sharp increase in temperatures toward lower $CH_4/O_2$ ratios is observed at a $CH_4/O_2$ ratio of 1.2 in steady state and at a $CH_4/O_2$ ratio of 1.4 in RFR operation.

The selectivity/conversion and temperature curves for both RFR and steady-state operation can be explained by two opposing effects of decreasing $CH_4/O_2$ ratios ($<2.0$) on the reaction mechanism: stoichiometrically, the highly exothermic combustion of methane is increasingly favored, which results in decreasing syngas selectivities and increasing temperatures. However, at the same time, increasing temperatures shift the reaction equilibrium toward the less exothermic partial oxidation of methane. As a consequence of the superpositioning of these two effects, maximum syngas selectivities are observed at $CH_4/O_2$ ratios lower than the stoichiometric point of 2.0, whereas temperatures remain constant over a broad range of $CH_4/O_2$ ratios.[21] The shift in maximum attainable syngas yields

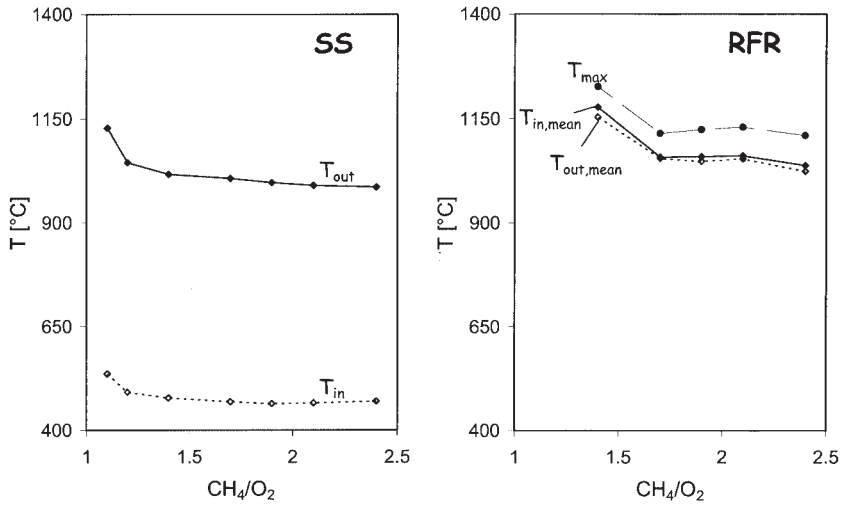


**Figure 8. Temperatures as a function of the $CH_4/O_2$ ratio.**

Steady-state (left) and RFR (right) operation. $\dot{V} = 4$ slm, $\tau/2 = 15$ s.

toward $CH_4/O_2$ ratios $< 2.0$ thus reflects the fact that the reactor operates under nonoptimal conditions. The observation that, in RFR operation, maximum $H_2$ selectivities are shifted toward higher $CH_4/O_2$ ratios compared to the steady-state process (Figure 7) is thus an indication of improved process efficiency.

The integrated heat exchange in the RFR results in increased catalyst temperatures when compared to a process without heat integration, as can generally be seen from higher temperatures in Figure 8. This temperature increase is particularly pronounced at the catalyst front edge. The strongly increased feed gas temperatures effectively reduce total oxidation of methane at the catalyst entrance and result in the observed pronounced increase in syngas yields compared to those of conventional reactor operation.

It seems remarkable that in contrast to catalyst entrance temperatures, averaged exit gas temperatures as well as maximum temperatures do not increase significantly from steady-state to reverse-flow operation. Although the irregular foam structure of the catalyst support precludes temperature measurements inside the catalyst, we can bound the maximum possible catalyst temperatures to a maximum of 1500°C, which is the melting point of the alumina foam. Unacceptable maximum temperatures are thus clearly avoided during the reactor operation. This is again indicative that this reactor configuration results in a true heat *integration* (that is, reactor temperatures are not simply increased with respect to steady-state operation), but the "regenerated" heat is kept in the catalyst zone and instantaneously converted into increased process yields.

### *Variation of the cycling period*

The semicycling period $\tau/2$ is a unique operating parameter of the dynamic reverse-flow reactor. It sets the time frame during which heat is stored and removed in the inert zones on both sides of the catalyst bed, and thus has a decisive influence on temperature profiles along the reactor axis. Two limiting cases can be distinguished a priori: (1) $\tau/2 \rightarrow \infty$ (that is, infinitely slow flow reversal), which corresponds to a transition to the conventional steady-state process without heat integration; and (2) $\tau/2 \rightarrow 0$ (that is, infinitely fast flow reversal), where the gas-flow stagnates and the reaction extinguishes. Thus, an optimum cycling time must exist between these two extremes.

This was tested experimentally by measuring syngas yields as a function of the cycling period. Results are shown in Figure 9 ($\dot{V} = 4$ slm, $CH_4/O_2 = 2.0$). Methane conversions and partial oxidation selectivities (left graph) show a maximum at a semicycling period of about 10 s. Mean catalyst temperatures (right graph) show a maximum around $\tau/2 = 5$–10 s ($T = 1100$°C), whereas maximum temperatures show a broad maximum centered around $\tau/2 = 10$ s and vary only within 30°C over the whole range of cycling periods investigated ($T = 1120$–1150°C).

At a flow rate of 4 slm, optimal heat integration obviously occurs at a cycling period $\tau/2 \approx 10$ s, as reflected in the maxima in syngas yields and mean reactor temperatures. Compared to large-scale industrial processes, where cycling times are usually in the range of minutes to hours, these are very short cycling periods, as can be expected from the fast kinetics and very compact reactors. High throughputs attainable in high-temperature catalytic reactions result in high convective heat transport and therefore lead to a fast cooling of the heat reservoirs, which are comparatively small because of the compact reactor size. This effect is further enhanced in our setup by the low thermal capacity and density of the cordierite inert zones used in the experiments, which prevents the accumulation of large amounts of heat. As a result, short optimum cycling periods are observed in the experimental setup used. Although cordierite extruded monoliths were used as heat reservoirs because of their ready availability, replacement of cordierite with higher-heat–capacity materials (such as alumina monoliths) is a simple way to improve the process.

It again seems noteworthy that maximum temperatures stay within a very narrow range throughout the experimentally tested range of operation parameters. This is an important point regarding catalyst stability as well as overall reactor stability, which typically degrade at exponentially increasing rate with increasing temperatures. The rather low maximum temperatures and weak dependency of these temperatures on cycling

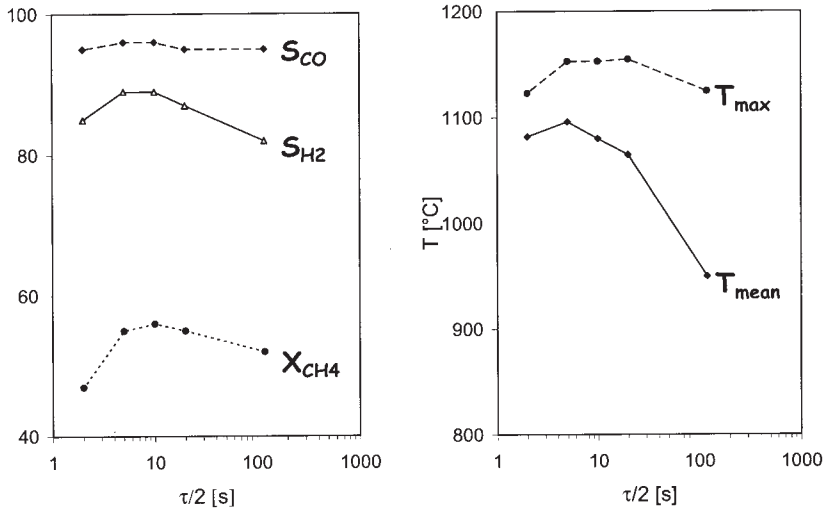


**Figure 9. CO selectivities ($S_{CO}$, dashed line), $H_2$ selectivities ($S_{H2}$, solid line), and $CH_4$ conversions ($X_{CH4}$, dotted line, left) as well as maximum ($T_{max}$, dotted line) and mean temperatures ($T_{mean}$, solid line; right) as a function of the cycling period $\tau/2$.**

$\dot{V}$ = 4 slm, $CH_4/O_2$ = 2.0.

frequency observed in the experiments thus indicate that cycling frequency can be optimized in this system without regard to catalyst or reactor stability issues.

### *Variation of reactor throughput*

One of the major advantages in high-temperature catalysis is the very high reaction rates that allow for high space–time yields and compact reactors. The influence of space–time onto reactor performance in dynamic and steady-state operation was investigated in another set of experiments by measuring syngas yields as a function of the volumetric gas flow rate. Volumetric flow rates between 1 and 5 slm were investigated, corresponding to catalyst residence times between 25 and 5 ms.

Figure 10 shows methane conversions and syngas selectivities with varying flow rate $\dot{V}$ for the RFR and the steady-state (SS) process ($CH_4/O_2$ = 2.0, $\tau/2$ = 15 s). Again, dynamic reactor operation leads to a pronounced increase in syngas yields compared to those of conventional reactor operation for flow rates in excess of 1 slm where yields are essentially identical. Furthermore, whereas syngas yields in the conventional process exhibit a maximum at 3 slm, partial oxidation selectivities as well as methane conversions increase continuously in the RFR over the whole range of flow rates investigated. Obviously, maximum attainable syngas yields are shifted toward even higher flow rates and thus even shorter contact times in dynamic reactor operation.

This behavior can be understood based on the changes in catalyst entrance and exit temperatures with varying flow rates

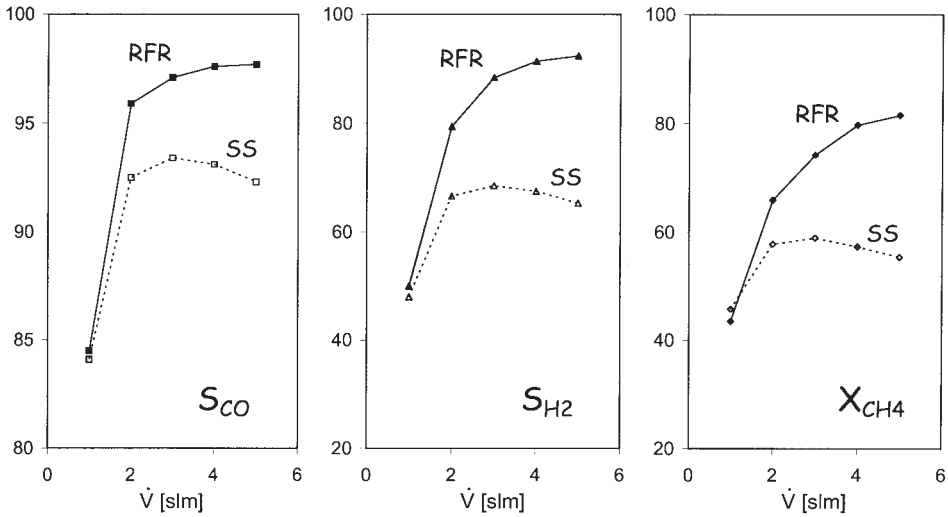


**Figure 10. CO selectivities ($S_{CO}$, left), $H_2$ selectivities ($S_{H2}$, middle), and $CH_4$ conversions ($X_{CH4}$, right) as a function of the total volumetric gas flow $\dot{V}$** for steady-state (SS, dotted lines) and RFR (solid lines) operation.

$CH_4/O_2$ = 2.0, $\tau/2$ = 15 s.

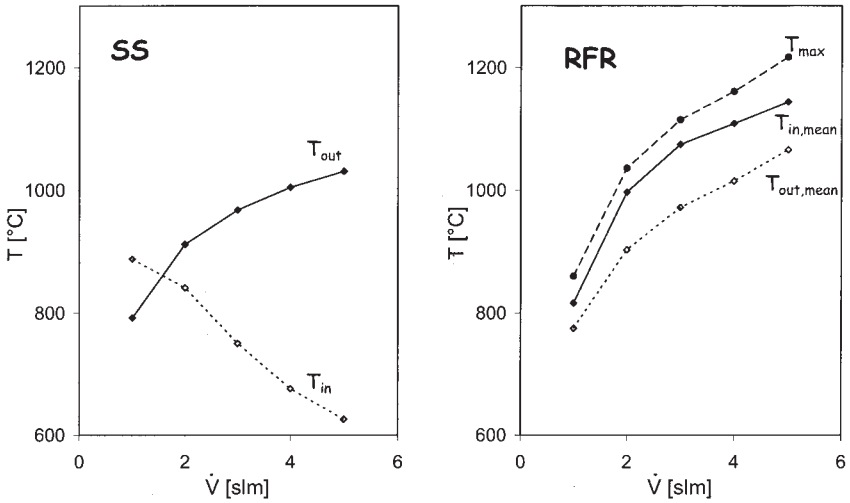


**Figure 11. Catalyst temperatures as a function of the total volumetric gas flow $\dot{V}$.**

Left: steady-state (SS) reactor ($T_{out}$: solid line; $T_{in}$: dashed line), right: RFR ($T_{max}$: dashed line; $T_{in,mean}$: solid line; $T_{out,mean}$: dotted line); $CH_4/O_2 = 2.0$, $\tau/2 = 15$ s.

as shown in Figure 11. In the conventional process, an increase in throughput leads to decreasing catalyst entrance and increasing catalyst exit temperatures, resulting in a scissorlike shape of these two temperature curves. In RFR operation, mean and maximum temperatures increase continuously with higher flow rates and run parallel to catalyst exit temperatures of the steady-state process.

Increasing the flow rate in the conventional process has two opposing effects on temperature profiles and therefore reaction selectivities: On one hand, it leads to an increase of heat generated by the reaction because more reactants are converted per unit time. This results in elevated catalyst temperatures—as can be seen from increasing catalyst exit temperature with higher flow rates—and is therefore favorable for syngas yields. On the other hand, however, increasing the flow rate leads to higher convective heat transport and increased amounts of cold feed gases impinging on the catalyst front edge. This results in a shift of the reaction front further into the catalyst bed and a decrease of the catalyst entrance temperature, thus thermodynamically favoring total oxidation of methane in this zone as also previously seen by Witt and Schmidt.[22] These two competing effects result in maximum selectivities and conversions at a flow rate of 3 slm in the conventional steady-state process.

Conversely, in RFR operation mean catalyst entrance temperatures increase continuously with higher flow rates, parallel to the exit temperatures of the steady-state process. To rationalize this behavior, we qualitatively investigated the thermal dynamics of the RFR using thermocamera measurements. Figure 12 shows thermocamera scans along the reactor axis, which were recorded at flow rates varying from 1 to 4 slm. The catalyst is positioned between about $z = 110$ and 120 mm. The curves represent nonnormalized temperature differences ($\Delta\theta$) between maximum and time-averaged temperatures of a full cycle. Clearly, $\Delta\theta$ increases substantially with higher flow rates and a much larger part of the inert zone is used for heat exchange. The amount of sensible heat accumulated in the inert zone is proportional to $\Delta\theta$ (given that $dH = c_p dT$) and therefore increases in the same direction. Because more heat is available, regenerative heat exchange thus results in a continuous increase in temperature level with higher flow rates, as observed in Figure 11. The detrimental effect (on syngas yields) of decreasing catalyst entrance temperatures with increasing flow rate, as observed in the conventional process, thus does not occur in the RFR. Instead, syngas yields continuously increase with higher throughputs. Obviously, this increase will not continue indefinitely because the capacity of the heat reservoir will set an upper limit to the continuous increase in heat regeneration. Our experimental setup was limited to maximum flow rates of 5 slm, and from the shape of the curves in Figure 10 it appears that selectivities and conversions are starting to level out at this point in our experiment. However, as mentioned earlier, the capacity of the heat reservoirs (the inert zones) could be significantly increased through the use of higher-heat–capacity materials, and thus significantly higher flow rates (that is, even shorter contact times) with further improved process yields should be attainable in this process.

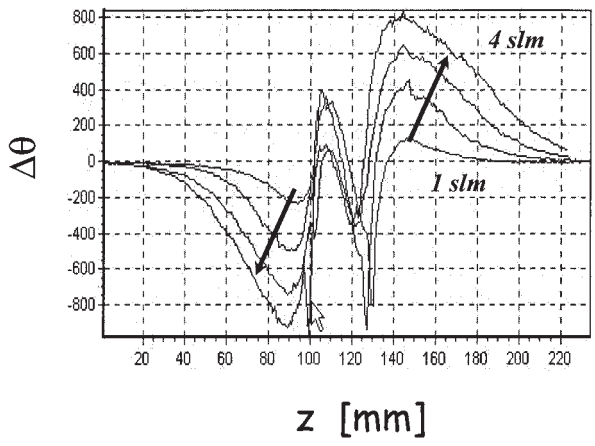


**Figure 12. Thermocamera scans with varying flow rates.**

Temperature differences (not normalized) between maximum and time-averaged temperatures of a full cycle along the reactor axis $z$ (the catalyst is positioned between $z = 110$ and $z = 120$ mm).

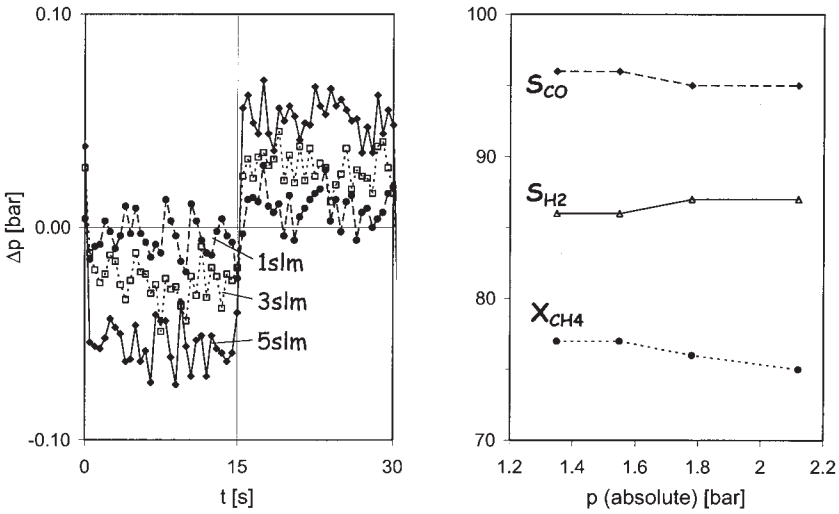


**Figure 13. Pressure drop across the reactor for 1 (circles), 3 (squares), and 5 (diamonds) slm during two semicycles (left graph), and mean syngas selectivities ($S_{CO}$: dashed line, $S_{H2}$: solid line) and $CH_4$ conversions ($X_{CH4}$, dotted line; right) as a function of the absolute pressure.**

$CH_4/O_2 = 2.0$, $\dot{V} = 4$ slm, $\tau/2 = 15$ s.

### *Variation of reactor pressure*

The absolute pressure inside the reactor is strongly dependent on the flow rate resulting from the experimental setup (that is, relatively long and thin capillaries between the reactor and the GC). For flow rates between 1 and 5 slm, the absolute pressure inside the reactor varies between 1.2 and 2.2 bar. To ensure that differences in selectivities and conversions with a variation of the flow rate do not occur because of differences in pressure, the influence of absolute pressure inside the reactor on syngas yields was investigated. Regulation of absolute pressure was accomplished by installing a needle valve into the RFR system immediately behind the point where the product gas streams are combined. Opening the valve resulted in a reduction of the absolute pressure inside the reactor.

Figure 13 shows the progression of pressure drop across the reactor at flow rates of 1, 3, and 5 slm during two semicycles (left graph) as well as mean syngas selectivities and methane conversions as a function of the absolute pressure inside the reactor ($\dot{V} = 4$ slm, $\tau/2 = 15$ s, $CH_4/O_2 = 2.0$, right graph).

The pressure drop across the reactor length increases with higher flow rates but stays well below 0.1 bar. Such low pressure drops constitute one of the main advantages of monolith systems because of their open structure (>80% porosity).

As seen in the right-hand graph in Figure 13, CO and $H_2$ selectivities as well as $CH_4$ conversions remain essentially constant within experimental error (±2%) over the range of pressures investigated. The pronounced differences in syngas yields with a variation of the flow rate therefore do not arise because of differences in absolute pressure inside the reactor but are exclusively a result of the increased utilization of the heat reservoirs represented by the inert zones.

Although our experimental setup did not allow us to go to significantly increased process pressures, Schmidt and coworkers[23-25] as well as our own work has shown in experimental and simulation studies of steady-state CPOM that increased reactor pressures should not result in significant contributions from homogeneous reactions (and thus in yield losses) up to reactor pressures of about 20 bar.

## Discussion

### *Reactor temperatures and syngas yields*

The results from our investigation of catalytic partial oxidation of methane over a Pt catalyst in a laboratory-scale reverse-flow reactor demonstrate that the integrated regenerative heat exchange in a RFR leads to strongly increased $CH_4$ conversions and syngas selectivities compared to results at conventional steady-state operation. This improvement is the direct result of an increase in catalyst entrance temperatures and advantageous temperature profiles along the reactor axis in the RFR because catalyst temperatures have a determining influence on syngas yields in this reaction system. Because of differences in reaction enthalpies for the two competing reaction pathways ($\Delta H_r = -800$ kJ/mol for total oxidation and $\Delta H_r = -37$ kJ/mol for partial oxidation of methane), low temperatures thermodynamically result in a preferential combustion of methane, which is therefore detrimental for syngas selectivities.

Although in steady-state reactor operation catalyst exit temperatures are generally very high, catalyst entrance temperatures are much lower and decrease substantially with increasing flow rates, thus favoring total oxidation of methane in the front section of the catalyst bed.[22] The temperature at the catalyst entrance is mainly influenced by convective cooling of the reactants as well as thermal conductivity of the catalyst. Hohn and Schmidt[25] showed that, by using alumina spheres rather than alumina foam monolith as a support, one can influence the heat-transport properties of the system and effectively increase syngas yields at high space velocities over Rh catalysts. Dynamic reactor operation on the contrary leads to a strong increase in catalyst entrance temperatures attributed to efficient regenerative heat exchange. Therefore, total oxidation is re-

duced and syngas yields improved compared to conventional reactor operation. Enhancements in selectivities and conversions can in all cases be explained by advantageous temperature profiles in the RFR throughout the experiments performed.

The classical application of a dynamic RFR is closely related to the phenomenon of a moving reaction front.[9] In a weakly exothermic reaction, the heat released is not sufficient to keep the reaction ignited so that the reaction front moves along the catalyst bed. The front part of the catalyst bed acts as a regenerative heat exchanger and heats up the cold feed gas while the reaction front creeps toward the exit of the reactor. To prevent the reaction from extinguishing once the reaction front reaches the outlet of the reactor, the flow through the reaction tube is reversed and the reaction front moves in the opposite direction.

In the current reaction system, which is characterized by the extremely high reaction rates of high-temperature catalysis, our experiments give no indication that the reaction front ever moves significantly away from the front edge of the catalyst. In fact, the differences between the RFR results and the steady-state operation during variation of the total gas flow rate seem to indicate that the very fact that the reaction front remains pinned to the catalyst front edge in reverse-flow operation is responsible to a large degree for the observed process improvements. As confirmed by thermocamera observations, the reaction front "jumps" on flow reversal virtually instantaneously from one end of the catalyst to the opposite end, whereas a slow thermal front moves along the inert zones, emptying and filling the upstream and downstream heat reservoirs, respectively.

### *Converting sensible heat into chemical energy*

As described above, the RFR principle is based on the idea of integrating sensible heat released by an exothermic reaction to increase catalyst temperatures. Although in the "classical" application of the RFR for waste gas combustion, this heat integration thus allows autothermal reactor operation, even for gas mixtures with an extremely low adiabatic temperature increase (down to $\Delta T \sim 15$ K),[26] in the current system the result of the heat integration is quite different: the additional heat fed back to the system is (to some extent) converted into chemical energy, as observed in the form of an increase in syngas yields rather than increased reactor temperatures. However, because of heat losses and both reactor and kinetic limitations, not all of the sensible heat is eventually converted into chemical energy. To characterize the system, it is helpful to estimate the efficiency $\eta$ of the dynamic heat integration. We therefore performed some basic calculations on the presented data to estimate how much of the sensible heat is ultimately converted into chemical energy.

Figure 14 shows a (standard) enthalpy vs. temperature plot to schematically illustrate the calculations described in the following. The enthalpy of the product gases is described (as usual) by $H = H^{\theta} + Cp\,\Delta T$, and can thus be separated into the "latent heat" of the gases, $H^{\theta}$, and the "sensible heat," that is, $Cp\,\Delta T$ (where $\Delta T = T - T^{\theta}$). In the steady-state process, products exit the catalyst bed at a high temperature ($T_{\text{catalyst-exit,SS}}$) and a relatively low standard enthalpy ($H^{\theta}_{\text{SS}}$). In comparison, the products of the RFR process exit the reactor at a low temperature ($T_{\text{reactor-exit,RFR}}$) and a higher enthalpy be-

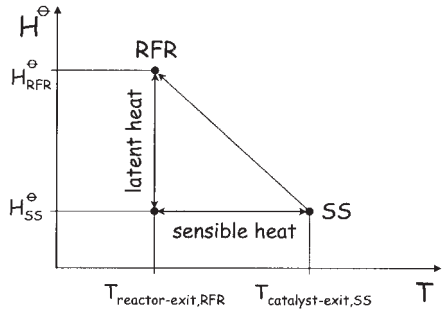


**Figure 14. Schematic diagram of standard enthalpy $H^{\theta}$ vs. temperature $T$, illustrating the conversion of sensible heat into latent heat in the RFR.**

cause of increased syngas yields ($H^{\theta}_{\text{RFR}}$). The difference between $T_{\text{catalyst-exit,SS}}$ and $T_{\text{reactor-exit,RFR}}$ is then proportional to the amount of sensible heat available for heat integration in the RFR (with the proportionality factor being the mixture-averaged heat capacity of the gases). On the other hand, the difference between the enthalpies of the steady-state and the RFR process at temperature $T_{\text{reactor-exit,RFR}}$ is equal to the difference in latent heat of the product gases (that is, the difference in chemical energy).

The enthalpy flow (of sensible heat) is thus calculated by the following

$$\dot{H}_{sh} = \sum_i \dot{n}_{i,\text{SS}}(c_{p,i}T_{\text{catalyst-exit,SS}} - c_{p,i}T_{\text{reactor-exit,RFR}}) \qquad (1)$$

where $\dot{H}_{sh}$ is the flow of sensible heat, $\dot{n}_{i,\text{SS}}$ is the molar flow of component $i$ of the steady-state process, $c_{p,i}$ is the temperature-dependent heat capacity of species $i$, $T_{\text{catalyst-exit,SS}}$ is the temperature at the catalyst exit in the steady-state process, and $T_{\text{reactor-exit,RFR}}$ is the temperature at the reactor exit in the RFR. $\Delta\dot{H}_{sh}$ thus represents the maximum amount of enthalpy per unit time, which can be integrated in the RFR system.

Differences in latent heat between product gases of the RFR and the steady-state process are calculated with the respective product gas compositions at the exit temperature of the reactor in dynamic operation. This difference therefore represents the amount of enthalpy that was converted into "chemical energy" in the RFR. Again, enthalpies are expressed as enthalpy flows by multiplying the enthalpy of species $i$ with the molar flow, yielding

$$\Delta\dot{H}_{\text{RFR-SS}} = \sum_i \dot{n}_{i,\text{RFR}}H_i(T_{\text{reactor-exit,RFR}}) - \sum_i \dot{n}_{i,\text{SS}}H_i(T_{\text{reactor-exit,RFR}}) \qquad (2)$$

where $\Delta\dot{H}_{\text{RFR-SS}}$ is the difference in enthalpy flow between RFR and steady-state operation, $\dot{n}_{i,\text{RFR}}$ is the molar flow of the RFR product gas component $i$, and $H_i$ is the enthalpy of species $i$ at temperature $T$.

The efficiency $\eta$ of converting sensible heat into chemical energy through regenerative heat exchange is calculated by dividing the two enthalpy flows

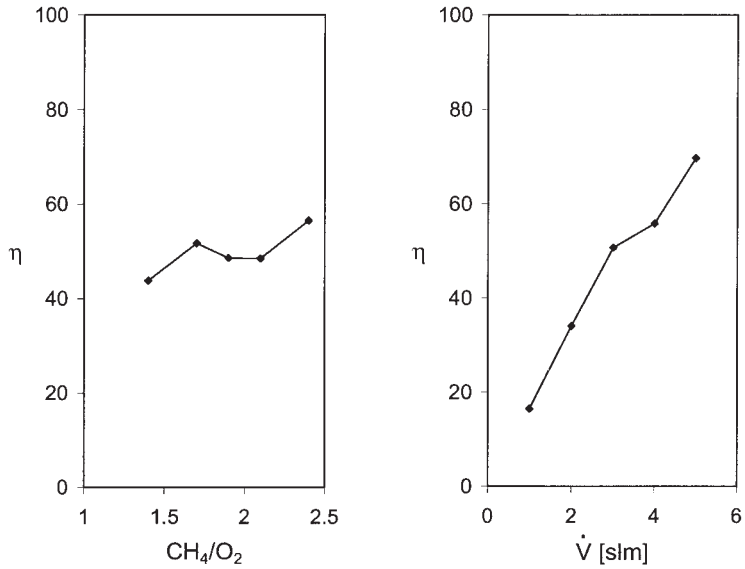


**Figure 15. Efficiency of heat integration $\eta$ in the RFR as a function of the $CH_4/O_2$ ratio ($\dot{V}$ = 4 slm, $\tau/2$ = 15 s, left graph) and the flow rate ($CH_4/O_2$ = 2.0, $\tau/2$ = 15 s, right graph).**

$$\eta = \frac{\Delta \dot{H}_{\mathrm{RFR-SS}}}{\dot{H}_{sh}} \tag{3}$$

This is a conservative approximation, given that the sensible heat enthalpy flow does not take heat losses to the surrounding into account, which occur in the laboratory-scale reactor. These heat losses reduce $T_{\mathrm{reactor-exit,RFR}}$ and increase $\dot{H}_{sh}$ above values if heat losses were accounted for, thus reducing the overall efficiency.

Using the above equations and experimental data, efficiencies were calculated as a function of $CH_4/O_2$ ratio and feed gas flow rate. Results are shown in Figure 15.

A variation of the $CH_4/O_2$ ratio (Figure 15, left graph) has very little influence on process efficiency, which remains almost constant at about 50% over the range investigated. This is in agreement with yield (Figure 7) and temperature (Figure 8) curves, which run parallel for steady-state and RFR operations. However, because maximum $H_2$ selectivities are shifted toward higher $CH_4/O_2$ ratios in the RFR compared to the conventional reactor, and thus also decrease at a higher $CH_4/O_2$ ratio (of 1.4), a slight reduction in process efficiency is observed at low $CH_4/O_2$ ratios.

Variation of the flow rate, on the other hand, has a very pronounced effect on process efficiency, which increases from $<$20% at a flow rate of 1 slm to $>$70% at 5 slm. This correlates well with results presented earlier, where thermocamera measurements (Figure 12) demonstrated that at higher flow rates a much larger portion of the inert zone is used for regenerative heat exchange. This increased use of the heat reservoirs is thus reflected in a pronounced increase in process efficiency. Overall, these results clearly emphasize that high flow rates are not only beneficial for high syngas yields, but are in fact necessary for efficient process operation.

## Summary and Conclusions

We presented results from a detailed investigation of catalytic partial oxidation of methane in a reverse-flow reactor. The reaction system is characterized by extreme temperatures and a complex interplay between partial and total oxidation reactions that limits attainable syngas yields at autothermal conditions. These limitations can be overcome by integrating the sensible heat of the product gases through heat integration in a multifunctional reactor concept. The efficient regenerative heat exchange in an RFR makes this reactor configuration particularly interesting for CPOM.

It was shown that RFR operation leads to substantially increased catalyst entrance temperatures compared to conventional steady-state reactor operation. These increased catalyst entrance temperatures efficiently reduce total oxidation of methane and result in a pronounced increase in syngas yields.

Variation of the reactor throughput (that is, gas flow rate) revealed that maximum attainable syngas yields are shifted toward higher flow rates and thus allow for even shorter contact times or higher space–time yields in reverse-flow operation. Increasing flow rates resulted in a strong increase in efficiency of the heat integration as a result of a more efficient use of the heat reservoirs represented by the inert zones. Although finding maximum possible syngas yields was not the aim of this study, even higher gas flow rates and inert zones with increased heat capacities could be identified as main parameters for process optimization, leaving room for further quantitative improvements of the described process.

Overall, extremely high space–time yields and very efficient regenerative heat integration make this reactor configuration particularly interesting for small-scale, decentralized or mobile syngas (and/or hydrogen) production, particularly because the required compact reactors for such applications will show increased heat losses and thus heat integration will be imperative for an economic and efficient small-scale process. Finally, it should be noted that the general conclusions from this study should also hold for related high-temperature processes, such as the oxidative dehydrogenation of higher alkanes to olefins,[27] and the presented studies are currently being extended to these reaction systems.

## Acknowledgments

Financial support by the German Science Foundation (DFG) as well as the Fund of the Chemical Industry (FCI) is gratefully acknowledged. Furthermore, we thank J. Scheidtmann for helpful assistance with the thermocamera measurements.

## Literature Cited

1. Hart D. Sustainable energy conversion: fuel cells—the competitive option? *Journal of Power Sources*, 2000;86:23–27.
2. Chum HL, Overend RP. Biomass and renewable fuels. *Fuel Processing Technology*. 2001;71:187–195.
3. Lee S-Y, Holder GD. Methane hydrates potential as a future energy source. *Fuel Processing Technology*. 2001;71:181–186.
4. Lunsfort JH. Catalytic conversion of methane to more useful chemicals and fuels: A challenge for the 21st century. *Catalysis Today*. 2000;63:165–174.
5. Wender I. Reactions of synthesis gas. *Fuel Processing Technology*. 1996;48:189–297.
6. Hickman DA, Schmidt LD. Production of syngas by direct catalytic oxidation of methane. *Science*. 1993;259:343–346.
7. Hickman DA, Schmidt LD. Syngas production by direct oxidation of methane on monoliths. *Journal of Catalysis*. 1992;138:267–282.
8. Agar DW. Multifunctional reactors: old preconceptions and new dimensions. *Chemical Engineering Science*. 1999;54:1299–1305.
9. Kolios G, Frauhammer J, Eigenberger G. Autothermal fixed-bed reactor concepts. *Chemical Engineering Science*. 2000;55:5945–5967.
10. Friedle U, Veser G. Counter-current heat-exchange reactor for high temperature partial oxidation reactions. *Chemical Engineering Science*. 1999;54:1325–1332.
11. Boreskov GK, Matros YS. Flow reversal of reaction mixture in a fixed catalyst bed—A way to increase the efficiency of chemical processes. *Applied Catalysis.* 1983;5:337–343.
12. Boreskov G, Matros Y. Unsteady-state performance of heterogeneous catalytic reactions. *Catalysis Reviews—Science and Engineering*. 1983;25:551–578.
13. Matros Y, Bunimovich G. Reverse-flow operation in fixed bed catalytic reactors. *Catalysis Reviews—Science and Engineering*. 1996;38: 1–68.
14. Eigenberger G, Nieken U. Catalytic combustion with periodic flow reversal. *Chemical Engineering Science*. 1988;43:2109–2115.
15. Nieken U, Kolios G, Eigenberger G. Fixed-bed reactors with periodic flow reversal: Experimental results for catalytic combustion. *Catalysis Today*. 1994;20:335–350.
16. Kolios G, Eigenberger G. Styrene synthesis in a reverse-flow reactor. *Chemical Engineering Science*. 1999;54:2637–2646.
17. Blanks RF, Wittrig TS, Petersen DA. Bidirectional adiabatic synthesis gas generator. *Chemical Engineering Science*. 1990;45:2407–2413.
18. de Groote AM, Froment GF. Synthesis gas production from natural gas in a fixed bed reactor with reversed flow. *Canadian Journal of Chemical Engineering*. 1996;74:735–741.
19. Gosiewski K, Bartmann U, Moszczynski M, Mleczko L. Effect of the intraparticle mass transport limitations on temperature profiles and catalytic performance of the reverse-flow reactor for the partial oxidation of methane to synthesis gas. *Chemical Engineering Science*. 1999;54:4589–4595.
20. Gosiewski K. Simulations of non-stationary reactors for the catalytic conversion of methane to synthesis gas. *Chemical Engineering Science*. 2001;56:1501–1510.
21. Veser G, Frauhammer J. Modelling steady state and ignition during catalytic methane oxidation in a monolith reactor. *Chemical Engineering Science*. 2000;55:2271–2286.
22. Witt PM, Schmidt LD. Effect of flow rate on the partial oxidation of methane and ethane. *Journal of Catalysis*. 1996;163:465–475.
23. Dietz AG, Schmidt LD. Effect of pressure on 3 catalytic partial oxidation reactions at millisecond contact times. *Catalysis Letters*. 1995;33:15–29.
24. Goralski CT Jr, RP O'Connor, Schmidt LD. Modeling homogeneous and heterogeneous chemistry in the production of syngas from methane. *Chemical Engineering Science*. 2000;55:1357–1370.
25. Hohn KL, Schmidt LD. Partial oxidation of methane to syngas at high space velocities over Rh-coated spheres. *Applied Catalysis A*. 2001; 211:53–68.
26. Eigenberger G. Fixed bed reactors. In: Schulz G, ed. *Ullmann's Encyclopedia of Industrial Chemistry.* B4, New York, NY: Wiley–VCH; 1992.
27. Bodke AS, Olschki DA, Schmidt LD Ranzi E. High selectivities to ethylene by partial oxidation of ethane. *Science*. 1999;285:712–715.

*Manuscript received Aug. 1, 2003, and revision received Apr. 23, 2004.*